Rapid Communications | Editors' Suggestion

Internal screening and dielectric engineering in magic-angle twisted bilayer graphene

J. M. Pizarro,[1,2,*] M. Rösner,[3] R. Thomale,[4] R. Valentí,[5] and T. O. Wehling[1,2,†]

[1]*Institute for Theoretical Physics, University of Bremen, Otto-Hahn-Allee 1, D-28359 Bremen, Germany*
[2]*Bremen Center for Computational Material Sciences, University of Bremen, Am Fallturm 1a, D-28359 Bremen, Germany*
[3]*Institute for Molecules and Materials, Radbound University, NL-6525 AJ Nijmegen, The Netherlands*
[4]*Institute for Theoretical Physics and Astrophysics, University of Würzburg, Am Hubland, D-97074 Würzburg, Germany*
[5]*Institute of Theoretical Physics, Goethe University Frankfurt am Main, D-60438 Frankfurt am Main, Germany*

(Received 9 May 2019; published 3 October 2019)

Magic-angle twisted bilayer graphene (MA-tBLG) has appeared as a tunable testing ground to investigate the conspiracy of electronic interactions, band structure, and lattice degrees of freedom to yield exotic quantum many-body ground states in a two-dimensional (2D) Dirac material framework. While the impact of external parameters such as doping or magnetic field can be conveniently modified and analyzed, the all-surface nature of the quasi-2D electron gas combined with its intricate internal properties pose a challenging task to characterize the quintessential nature of the different insulating and superconducting states found in experiments. We analyze the interplay of internal screening and dielectric environment on the intrinsic electronic interaction profile of MA-tBLG. We find that interlayer coupling generically enhances the internal screening. The influence of the dielectric environment on the effective interaction strength depends decisively on the electronic state of MA-tBLG. Thus, we propose the experimental tailoring of the dielectric environment, e.g., by varying the capping layer composition and thickness, as a promising pursuit to provide further evidence for resolving the hidden nature of the quantum many-body states in MA-tBLG.

DOI: 10.1103/PhysRevB.100.161102

Introduction. Stacking two graphene layers at a twist angle θ on top of each other leads to twisted bilayer graphene (tBLG) featuring a moiré pattern with an intricate emergent low-energy electronic structure. For small twist angles $\theta < 2^\circ$, the resulting superlattices host several thousand atoms per unit cell. In this situation, the electronic bands around the charge neutrality point (CNP) become very flat [1,2], which facilitates strong correlation effects. Recent experiments [3–6] reported the emergence of possibly unconventional superconducting and insulating states in magic-angle tBLG (MA-tBLG) at different levels of doping. The insulating states occur for commensurate fillings at both electron and hole dopings [3,5,7], signaling a possible Mott-Hubbard origin [8–10]. Around these insulating states, superconductivity emerges [4,5,7], resembling the phase diagram of high-T_c cuprate superconductors [11,12] and other unconventional superconductors [13,14]. Different models [8–10,15–32] have been proposed to understand the physics behind these insulating and superconducting states.

Electronic correlations in ultrathin systems such as MA-tBLG depend decisively on the effective electron-electron interaction profile, which is determined by a delicate interplay of screening processes taking place in the dielectric environment and the material itself [33–35]. The profile of the effective electron-electron interactions presents a central uncertainty in the current understanding of MA-tBLG.

In this Rapid Communication, we provide a quantitative study of the internal polarizability and effects of the dielectric environment on the effective electron-electron interaction in MA-tBLG. We consider MA-tBLG in dielectric surroundings [see Figs. 1(a) and 1(b)], directly resembling different experimental setups: (a) MA-tBLG is separated by possible hexagonal boron nitride (hBN) encapsulation from a dielectric environment (ε_2) at distance d below and above. The case of a metallic gate at a certain distance d from MA-tBLG is included in this analysis for $\varepsilon_2 \to \infty$. (b) The special case of the dielectric ε_2 in direct contact with MA-tBLG as realized for $d = 3.35$ Å is shown. Our main findings are as follows: (1) Intrinsic screening in MA-tBLG is enhanced by interlayer coupling and is larger than previously assumed in the model of uncoupled graphene double layers [3,8,18,24,36–41]; (2) in a possible Mott insulating phase, the effective interaction can be modulated on the order of 50% by changing the dielectric environment; and (3) metallic states of MA-tBLG are mostly insensitive to the dielectric environment. Finally, a generically applicable, realistic, and yet simple model of the effective electron-electron interaction in MA-tBLG setups as depicted in Fig. 1 is provided.

Internal screening. As a first step, we calculate the intrinsic polarization function of MA-tBLG in the random phase approximation (RPA) using the low-energy continuum model for the electronic bands of tBLG from Refs. [2,8]. In this model [42], two sets of Dirac electron bands originating from the lower and the upper graphene layers hybridize due to the interlayer coupling, which is modulated with the periodicity of the moiré superlattice [cf. Fig. 1(c)]. In reciprocal space, there is correspondingly a coupling between Dirac electron

*jpizarro@uni-bremen.de
†twehling@uni-bremen.de

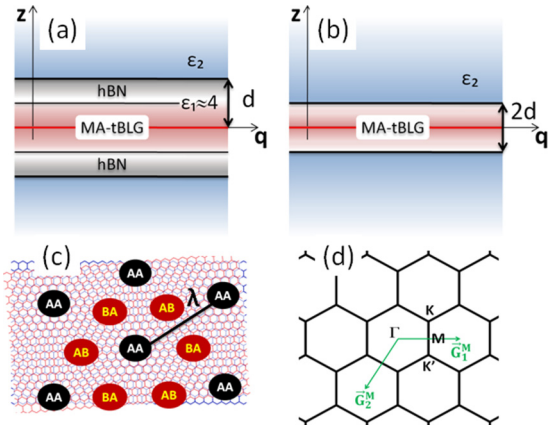

FIG. 1. Setups for dielectric engineering of MA-tBLG: (a) MA-tBLG encapsulated in hBN, where the dielectric function $\varepsilon_1 \approx 4$ encodes both the contribution from hBN (gray) and from the σ-band higher-energy background of MA-tBLG (red). ε_2 describes the dielectric surrounding (blue) at a distance d from the center of MA-tBLG. MA-tBLG with a metallic gate at a distance d is realized for $\varepsilon_2 \to \infty$. (b) Dielectric ε_2 in direct contact with MA-tBLG as described by $d = 3.35$ Å, which is the interlayer distance of BLG and hBN [34]. (c) In the moiré pattern of MA-tBLG, *AA* and *AB*/*BA* regions can be recognized according to the stacking of the atoms in each graphene layer. The moiré lattice constant λ corresponds to the distance between adjacent *AA* regions, and is 134 Å for the first magic angle. (d) The reciprocal space is broken up into the hexagonal mini Brillouin zones (BZs) associated with the moiré real-space superlattice. The reciprocal lattice is spanned by the reciprocal lattice vectors $\mathbf{G}_1^M$ and $\mathbf{G}_2^M$ [8]. Neighboring mini-BZs are included in the low-energy continuum description of MA-tBLG up to a certain cutoff G_c.

states at each $\mathbf{k}$ vector in one layer with states at $\mathbf{k}+\mathbf{G}$ in the other layer, where $\mathbf{G}$ is a reciprocal lattice vector associated with the moiré superlattice: $\mathbf{G} = m\mathbf{G}_1^M + n\mathbf{G}_2^M$ with m, n integers, and $\mathbf{G}_1^M$ and $\mathbf{G}_2^M$ spanning the reciprocal lattice of tBLG [see Fig. 1(d)]. Then, the electronic states of tBLG are expanded in terms of coupled two-dimensional Dirac spinors up to a certain plane-wave cutoff $G_c = 8G_M$, where $G_M = |\mathbf{G}_1^M| = |\mathbf{G}_2^M|$ [42]. MA-tBLG is then realized when the twisting angle is set to 1.05°.

In reciprocal space, the polarization operator Π_0 is a function of the scattering vector $\mathbf{q}$ and a matrix indexed by reciprocal lattice vectors $\mathbf{G}$ and $\mathbf{G}'$. At zero transferred frequency, Π_0 takes the form [43]

$$\Pi_0^{\mathbf{G},\mathbf{G}'}(\mathbf{q}) = \frac{g_s g_v}{S_M N} \sum_{\substack{\mathbf{k} \\ \alpha,\beta \\ \mathbf{G}_2,\mathbf{G}_2'}} \mathcal{M}^{\alpha\beta}_{\mathbf{G}_2,\mathbf{G}_2',\mathbf{G},\mathbf{G}'} \frac{f^\alpha_{\mathbf{k}} - f^\beta_{\mathbf{k}+\mathbf{q}}}{i\eta + E^\alpha_{\mathbf{k}} - E^\beta_{\mathbf{k}+\mathbf{q}}}. \tag{1}$$

Here, $g_s = g_v = 2$ are the spin and valley degeneracy factors, $S_M = \sqrt{3}\lambda^2/2$ is the moiré unit cell area, where $\lambda \approx 134$ Å is the moiré lattice constant, $N = 100$ is the number of $\mathbf{k}$ points, α and β encode the sublattice (A_1, B_1, A_2, and B_2) and band indices [42], $\mathbf{G}_2$, $\mathbf{G}_2'$, $\mathbf{G}$, and $\mathbf{G}'$ are reciprocal lattice vectors, $f^\alpha_{\mathbf{k}}$ and $E^\alpha_{\mathbf{k}}$ are, respectively, the Fermi function and the band energy of α at $\mathbf{k}$, $\eta = 0.5 \times 10^{-6}$–$10^{-8}$ eV is the broadening parameter, and we consider the temperature

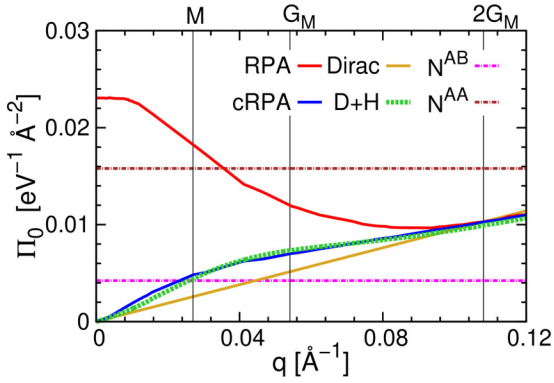

FIG. 2. Static polarization function of MA-tBLG in comparison to uncoupled tBLG (Π_0^{Dirac}, orange line) from Eq. (3), the model of quasilocalized states plus Dirac background ($\Pi_0^{\text{D+H}}$, green dashed line) from Eq. (4), and the DOS of commensurate *AA* (brown dashed-dotted line) and *AB* BLG (pink dashed-dotted line). For MA-tBLG, polarizabilities from RPA (red line) assuming a metallic state and cRPA (blue line), i.e., excluding polarization processes within the flat bands similarly to a Mott insulator, are shown. $G_M = 0.057$ Å^{-1} marks the length of the reciprocal lattice vectors.

$T \approx 50$ K (inverse temperature $\beta = 200\ \text{eV}^{-1}$) to calculate the Fermi functions f^α_k in Eq. (1) [42]. Π_0 is thus given in units of eV^{-1} Å^{-2}. The overlap matrix $\mathcal{M}$ results from the Dirac spinor plane-wave expansion coefficients $c^{\alpha,\mathbf{G}}_{\mathbf{k}}$ via

$$\mathcal{M}^{\alpha\beta}_{\mathbf{G}_2,\mathbf{G}_2',\mathbf{G},\mathbf{G}'} = \left(c^{\alpha,\mathbf{G}_2}_{\mathbf{k}}\right)^\dagger \left(c^{\beta,\mathbf{G}_2'-\mathbf{G}'}_{\mathbf{k}+\mathbf{q}}\right)^\dagger c^{\beta,\mathbf{G}_2'}_{\mathbf{k}+\mathbf{q}} c^{\alpha,\mathbf{G}+\mathbf{G}_2}_{\mathbf{k}}. \tag{2}$$

We then study the internal screening in MA-tBLG for two possible scenarios: first, screening according to the RPA, which assumes MA-tBLG to be in a conventional metallic state; second, a scenario resembling insulating states which are modeled within the so-called constrained RPA (cRPA) [44]. In the cRPA, polarization processes taking place inside the low-energy flat bands are excluded from Eq. (1) by setting $f^\alpha_{\mathbf{k}} = \frac{1}{2}$ for all states α from this low-energy sector. The resulting cRPA partially screened interactions are those which should be considered in effective Hamiltonians solely dealing with the low-energy flat bands, and correspond also to the screened interactions that would be expected if electronic correlations suppress low-energy polarization processes such as in a Mott insulator [45,46].

The results presented in the following are obtained at charge neutrality with the continuum model from Ref. [8] at a twist angle of $\theta = 1.05°$. We show in the Supplemental Material [42] that our results are robust against changes in twist angle, doping, and interlayer coupling parameters.

Figure 2 compares the RPA and cRPA polarization functions [42,47] for MA-tBLG to the case of uncoupled tBLG, where the interlayer coupling is neglected. Uncoupled tBLG hosts eight flavors of ideal Dirac fermions due to spin $g_s = 2$, valley $g_v = 2$, and layer degeneracy $g_l = 2$ resulting in a linearly-q-dependent polarization function [48],

$$\Pi_0^{\text{Dirac}}(q) = g_s g_v g_l \frac{q}{16\hbar v_F}, \tag{3}$$

where v_F is the Fermi velocity. For $q < G_M$, the intrinsic polarization functions of MA-tBLG, both in RPA and cRPA,

systematically exceed the uncoupled tBLG model. Intrinsic screening is thus significantly larger in MA-tBLG than previously assumed [3,8,18,24,36–41]. Only at larger momentum transfer $q \gtrsim 1.5G_M \approx 0.08$ Å^{-1}, the RPA and cRPA polarization functions of MA-tBLG approach values corresponding to the uncoupled model. This behavior can be understood from the interplay of intra- and interlayer coupling: At sufficiently large momentum transfer $q > G_M$, the intralayer coupling $\hbar v_F|q| \gtrsim 0.3$ eV dominates over the interlayer one. At $q < G_M$, however, the interlayer coupling cannot be neglected.

In the RPA model, i.e., in the metallic case, the enhancement of screening for $q < G_M$ is due to the high density of states (DOS) around the Fermi level originating from the flat bands. In the cRPA screening processes inside flat bands are excluded, which explains why the polarization function is smaller than in the RPA case. Still, the cRPA polarizability is clearly enhanced as compared to the uncoupled case for $q < G_M$. This can be understood as follows: While polarization processes taking place entirely inside the flat-band manifold are excluded in cRPA, gapped transitions between states associated with peaks in the DOS, e.g., between the flat bands and higher-energy states with corresponding peaks in the MA-tBLG DOS around $E \approx \pm 20$ meV and ± 60 meV [42], are possible. These gapped transitions are reminiscent of atomic systems. The hydrogen atom, as the simplest example, would yield a q-dependent polarizability of the form $\Pi_0^{\mathrm{H}}(q) \sim \frac{q^2}{[1+(\frac{q}{b})^2]^5}$ [49], where the parameter b is an effective inverse orbital radius. Superimposing this quasiatomic model Π_0^{H} with a Dirac electron background capturing all higher-energy processes leads to the ansatz,

$$\Pi_0^{\mathrm{D+H}}(q) = \Pi_0^{\mathrm{Dirac}}(q) + a\frac{q^2}{\left[1+\left(\frac{q}{b}\right)^2\right]^5}. \tag{4}$$

Figure 2 shows that Eq. (4) fits the cRPA numerics very well, upon choosing $a \approx 4.1$ eV^{-1} and $b \approx 0.088$ Å^{-1}. Thus, we suggest to use Eq. (4) for calculations of cRPA screened Coulomb interaction matrix elements in MA-tBLG.

While screening in MA-tBLG has been often approximated in terms of uncoupled tBLG [3,8,18,24,37–41], an alternative point of view is that MA-tBLG is a patchwork of *AA* and *AB* stacked bilayer graphene (BLG) regions. For $q \gtrsim G_M/2$ the MA-tBLG polarizability fits, indeed, into the range marked by the low-energy density of states (DOS) of *AA* BLG, $N^{AA}(E_F) = 0.0158$ eV^{-1} Å^{-2}, and *AB* BLG, $N^{AB}(E_F) = 0.0042$ eV^{-1} Å^{-2} [50]. Further below we show that the *AB* BLG model gives good estimates for the effective local interactions when compared with the cRPA. On physical grounds, our results for the polarization function show that MA-tBLG can be seen as a flat-band system embedded in an almost metallic background generated by the higher-energy bands, which are separated by approximately 15 meV from the low-energy flat bands [42].

Dielectric engineering. We now assess the possibilities for dielectric engineering of MA-tBLG in experimental setups as shown in Figs. 1(a) and 1(b). The screened interaction is

$$W(q) = \frac{V(q)}{\varepsilon(q)}, \tag{5}$$

where $V(q) = 2\pi e^2/q$ is the bare interaction and $\varepsilon(q) = \varepsilon_{\mathrm{env}}(q) + V(q)\Pi_0(q)$ is the dielectric function [48]. The latter accounts for the screening resulting from the electrons in the bands of MA-tBLG via $\Pi_0(q)$ plus the screening produced by the surrounding dielectrics and higher-energy bands of MA-tBLG summarized in $\varepsilon_{\mathrm{env}}(q)$. In the setups from Fig. 1, the background dielectric function reads [34]

$$\varepsilon_{\mathrm{env}}(q) = \varepsilon_1\frac{1-\tilde{\varepsilon}_2^2 e^{-4qd}}{(1+\tilde{\varepsilon}_2 e^{-2qd})^2}, \tag{6}$$

where we approximated $\varepsilon_1 \approx 4$ [48] and $\tilde{\varepsilon}_2 = (\varepsilon_1 - \varepsilon_2)/(\varepsilon_1 + \varepsilon_2)$. Together with the polarizability $\Pi_0(q)$ obtained either numerically in cRPA from Eq. (1) or conveniently from the fit of Eq. (4), Eqs. (5) and (6) specify the appropriately screened interaction of MA-tBLG in different dielectric surroundings, which should be incorporated in interacting electron models of the low-energy flat bands.

To illustrate the influence of the dielectric surrounding on the effective interaction in MA-tBLG in terms of a single descriptor, we consider an effective local interaction U obtained by a Fourier transformation of $W(q)$,

$$U = \int \frac{d^2\mathbf{q}}{(2\pi)^2} W(\mathbf{q}) = \int_0^{q_c} \frac{dq}{2\pi} qW(q). \tag{7}$$

Here, the cutoff q_c relates to the two-dimensional (2D) radial spread r_{WF} of the Wannier functions (WF) constructed from the MA-tBLG low-energy bands, $q_c \approx \pi/r_{\mathrm{WF}}$. We choose r_{WF} to be half of the moiré lattice constant λ, hence $q_c \approx 0.047$ Å^{-1}.

Figure 3(a) shows the influence of the dielectric environment ε_2 on U, where we assume that the surrounding dielectric is in direct contact with MA-tBLG [cf. Fig. 1(b)]. Assuming a metallic state of MA-tBLG as in the RPA model, the dielectric environment has barely any effects, and U remains almost constant around 10 meV. This insensitivity of metallic states in MA-tBLG to the dielectric surrounding is due to a high intrinsic polarizability which masks any environmental polarizabilities (cf. RPA curves in Fig. 2 and Fig. S3 of the Supplemental Material [42]).

On the other hand, the cRPA estimated U varies from 40 to ≈20 meV when ε_2 increases. Interestingly, 40 meV is approximately the splitting of the upper and lower Hubbard bands when a gap is opened at the CNP, as recently measured in scanning tunneling spectroscopy (STS) [6]. Besides its relevance for low-energy effective Hamiltonians, the cRPA solution resembles the fully screened interaction in certain insulating states, where screening from the low-energy states is suppressed. In this situation the dielectric environment can modify the effective interaction U up to ≈ 40%–50%.

The influence of the metallic gate ($\varepsilon_2 \to \infty$) at a distance d from MA-tBLG [cf. Fig. 1(b)] on the effective local interaction U is shown in Fig. 3(b). In an insulating state (cRPA case), the influence of the metallic gate is strong if

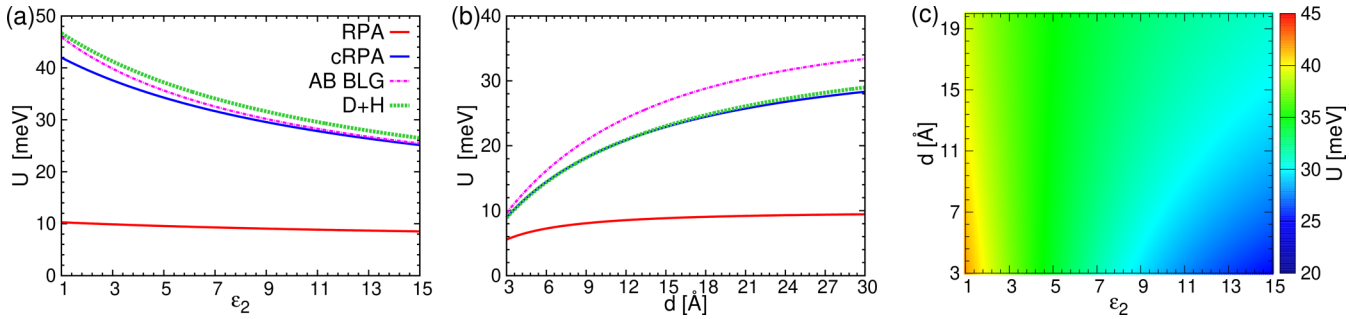

FIG. 3. Dielectric engineering of MA-tBLG with an external dielectric ε_2 at a distance d. (a) Effective local interaction U as a function of the dielectric constant ε_2 of the environment in direct contact with MA-tBLG. The RPA (red line) mimicking metallic screening and cRPA (blue line) numerical results assuming suppressed low-energy screening for MA-tBLG are compared with the analytical estimates from the *AB* BLG model (pink dashed-dotted line) and the quasiatomic model with a Dirac background (D + H, green dashed line) from Eq. (4). (b) Influence of a metallic gate ($\varepsilon_2 \to \infty$) at a distance d from MA-tBLG on U. (c) Effective cRPA screened local interaction U (color coded) as a function of the dielectric surrounding ε_2 and its distance d from MA-tBLG.

the distance from MA-tBLG is on the order of $d \lesssim 20$ Å. In this case, U is reduced by a factor of 2 when approaching the gate from $d \sim 30$ Å to $d \sim 10$ Å. The fact that the metallic gate has to be as close as $d \lesssim 20$ Å, which is much smaller than the moiré lattice constant (134 Å), in order to see any substantial effect on U even in the cRPA/insulating case is due to MA-tBLG being a flat-band system embedded in an already almost metallic background. In the RPA case, the metallic gate has again a much smaller effect on U. Only for metallic gates very close to MA-tBLG ($d \approx 3.35$ Å), U is reduced from 10 to 5 meV. Thus, in metallic states of MA-tBLG (RPA case), metallic gates can only influence the electron-electron interactions due to external screening if they are very close to the MA-tBLG, and a possible hBN spacer separating the gate from the MA-tBLG should be as thin as a monolayer. The dependence of the effective local cRPA screened interaction U on the dielectric surrounding ε_2 and its distance d from MA-tBLG is summarized in Fig. 3(c). U can be reduced from 40 meV (free-standing case) to 10 meV (strong screening environment) if the surrounding dielectric gets sufficiently close $d \lesssim 20$ Å.

Additionally to the RPA and cRPA numerics according to Eq. (1), we also propose simple approximate forms to calculate screened Coulomb interaction matrix elements. First, by choosing the expression of Eq. (4) for the polarizability, we reproduce also the effective cRPA screened local interaction quite accurately. Even more simplistically, Fig. 3 also shows that screening based on the DOS of *AB* BLG provides us with a good estimate for U in the cRPA case.

Summary. We have shown that the sensitivity of the interaction profile in MA-tBLG to the dielectric environment depends decisively on the quantum state of the electrons in the low-energy flat-band manifold. Currently, the nature of the insulating states at half filling, of superconductivity near half filling, and of the gaps measured in STS at charge neutrality are major open problems in the understanding of MA-tBLG. What would an experimentally detected significant influence of the dielectric surrounding on spectral, thermodynamic, or transport properties in any of these phases imply? Based on our results any strong influence of the external dielectric means that charge screening in the low-energy bands is substantially suppressed as compared to a conventional metallic state as assumed in RPA. That is hardly possible for insulating or any kind of ordered states resulting from a weak-coupling instability, which affect only a small sector of states in the vicinity of the noninteracting Fermi surface. Thus, the significant impact of external dielectrics on correlated insulating states implies that they are at strong coupling in the sense that states from the entire mini-BZ contribute significantly. Similarly, any impact of the dielectric surrounding on superconductivity implies strong-coupling physics at work, and possibly hints at an unconventional origin.

Currently, there are arguments in favor and against strong-coupling physics governing different parts of the MA-tBLG phase diagram. On the side in favor, is the ratio of effective interactions and bandwidth: In case of partial screening as described in cRPA, the effective interaction largely exceeds the bandwidth, which is suggestive of strong coupling. In line with a strong-coupling scenario, close to charge neutrality, STS further measured "gaps" on the scale of several 10 meV [6] and transport experiments reported suppression of conductance around charge neutrality being robust against temperature and magnetic fields [3,5,7]. At and around half filling, the situation is more complex: The generic shape of the phase diagram in this region appears to exhibit similarities to the cuprate high-T_c superconductors, which might be seen as an indication of favoring strong-coupling physics. At half filling, however, the insulating states are fragile, i.e., they are easily destroyed by magnetic fields ($B \sim 5$ T) and temperature ($T \sim 4$ K), in line with gaps that are small ($\Delta \sim 0.3$ meV) [3,5,7]. All these energies are at least an order of magnitude smaller than the expected width of the flat bands, and would be consistent with a weak-coupling scenario. Experimental studies of the response of MA-tBLG to changes in the surrounding dielectric will thus be useful to distinguish between strong- and weak-coupling scenarios, and to pinpoint the nature of the different quantum many-body states in MA-tBLG.

Acknowledgments. We thank D. A. Abanin, E. Bascones, and F. Guinea for useful conversations. J.M.P. and T.O.W. acknowledge funding from DFG-RTG 2247 (QM^3) and the European Graphene Flagship. R.T. is supported by DFG-SFB

1170 Tocotronics (Project B04), DFG-SPP 1666, and further acknowledges financial support from the DFG through the Würzburg-Dresden Cluster of Excellence on Complexity and Topology in Quantum Matter–*ct.qmat* (EXC 2147, Project No. 39085490). R.V. acknowledges funding from DFG-TRR 49.

[1] E. Suárez Morell, J. D. Correa, P. Vargas, M. Pacheco, and Z. Barticevic, Phys. Rev. B **82**, 121407(R) (2010).
[2] R. Bistritzer and A. H. MacDonald, Proc. Natl. Acad. Sci. USA **108**, 12233 (2011).
[3] Y. Cao, V. Fatemi, A. Demir, S. Fang, S. L. Tomarken, J. Y. Luo, J. D. Sanchez-Yamagishi, K. Watanabe, T. Taniguchi, E. Kaxiras *et al.*, Nature (London) **556**, 80 (2018).
[4] Y. Cao, V. Fatemi, S. Fang, K. Watanabe, T. Taniguchi, E. Kaxiras, and P. Jarillo-Herrero, Nature (London) **556**, 43 (2018).
[5] M. Yankowitz, S. Chen, H. Polshyn, Y. Zhang, K. Watanabe, T. Taniguchi, D. Graf, A. F. Young, and C. R. Dean, Science **363**, 1059 (2019).
[6] Y. Choi, J. Kemmer, Y. Peng, A. Thomson, H. Arora, R. Polski, Y. Zhang, H. Ren, J. Alicea, G. Refael *et al.*, Nat. Phys., (2019).
[7] X. Lu, P. Stepanov, W. Yang, M. Xie, M. A. Aamir, I. Das, C. Urgell, K. Watanabe, T. Taniguchi, G. Zhang *et al.*, arXiv:1903.06513.
[8] M. Koshino, N. F. Q. Yuan, T. Koretsune, M. Ochi, K. Kuroki, and L. Fu, Phys. Rev. X **8**, 031087 (2018).
[9] L. Rademaker and P. Mellado, Phys. Rev. B **98**, 235158 (2018).
[10] J. M. Pizarro, M. J. Calderón, and E. Bascones, J. Phys. Commun. **3**, 035024 (2019).
[11] B. Keimer, S. A. Kivelson, M. R. Norman, S. Uchida, and J. Zaanen, Nature (London) **518**, 179 (2015).
[12] A. Kordyuk, Low Temp. Phys. **41**, 319 (2015).
[13] Y. Kurosaki, Y. Shimizu, K. Miyagawa, K. Kanoda, and G. Saito, Phys. Rev. Lett. **95**, 177001 (2005).
[14] B. Sipos, A. F. Kusmartseva, A. Akrap, H. Berger, L. Forró, and E. Tutis, Nat. Mater. **7**, 960 (2008).
[15] H. C. Po, L. Zou, A. Vishwanath, and T. Senthil, Phys. Rev. X **8**, 031089 (2018).
[16] B. Roy and V. Juričić, Phys. Rev. B **99**, 121407(R) (2019).
[17] J. F. Dodaro, S. A. Kivelson, Y. Schattner, X. Q. Sun, and C. Wang, Phys. Rev. B **98**, 075154 (2018).
[18] C.-C. Liu, L.-D. Zhang, W.-Q. Chen, and F. Yang, Phys. Rev. Lett. **121**, 217001 (2018).
[19] D. M. Kennes, J. Lischner, and C. Karrasch, Phys. Rev. B **98**, 241407(R) (2018).
[20] H. Isobe, N. F. Q. Yuan, and L. Fu, Phys. Rev. X **8**, 041041 (2018).
[21] F. Wu, A. H. MacDonald, and I. Martin, Phys. Rev. Lett. **121**, 257001 (2018).
[22] A. Thomson, S. Chatterjee, S. Sachdev, and M. S. Scheurer, Phys. Rev. B **98**, 075109 (2018).
[23] M. Ochi, M. Koshino, and K. Kuroki, Phys. Rev. B **98**, 081102(R) (2018).
[24] F. Guinea and N. R. Walet, Proc. Natl. Acad. Sci. USA **115**, 13174 (2018).
[25] H. C. Po, L. Zou, T. Senthil, and A. Vishwanath, Phys. Rev. B **99**, 195455 (2019).
[26] E. Laksono, J. N. Leaw, A. Reaves, M. Singh, X. Wang, S. Adam, and X. Gu, Solid State Commun. **282**, 38 (2018).
[27] J. W. F. Venderbos and R. M. Fernandes, Phys. Rev. B **98**, 245103 (2018).
[28] Y. W. Choi and H. J. Choi, Phys. Rev. B **98**, 241412(R) (2018).
[29] V. Kozii, H. Isobe, J. W. F. Venderbos, and L. Fu, Phys. Rev. B **99**, 144507 (2019).
[30] J. Kang and O. Vafek, Phys. Rev. Lett. **122**, 246401 (2019).
[31] K. Seo, V. N. Kotov, and B. Uchoa, Phys. Rev. Lett. **122**, 246402 (2019).
[32] M. Xie and A. H. MacDonald, arXiv:1812.04213.
[33] T. O. Wehling, E. Şaşioğlu, C. Friedrich, A. I. Lichtenstein, M. I. Katsnelson, and S. Blügel, Phys. Rev. Lett. **106**, 236805 (2011).
[34] M. Rösner, E. Şaşioğlu, C. Friedrich, S. Blügel, and T. O. Wehling, Phys. Rev. B **92**, 085102 (2015).
[35] G. Schönhoff, M. Rösner, R. E. Groenewald, S. Haas, and T. O. Wehling, Phys. Rev. B **94**, 134504 (2016).
[36] T. Stauber and H. Kohler, Nano Lette. **16**, 6844 (2016).
[37] L. Zhang, Sci. Bull. **64**, 495 (2019).
[38] J. González and T. Stauber, Phys. Rev. Lett. **122**, 026801 (2019).
[39] A. O. Sboychakov, A. V. Rozhkov, A. L. Rakhmanov, and F. Nori, Phys. Rev. B **100**, 045111 (2019).
[40] Y. Fu, E. J. König, J. H. Wilson, Y.-Z. Chou, and J. H. Pixley, arXiv:1809.04604.
[41] J. González, F. Guinea, and M. A. H. Vozmediano, Phys. Rev. B **59**, R2474(R) (1999).
[42] See Supplemental Material at http://link.aps.org/supplemental/10.1103/PhysRevB.100.161102 for details of the low-energy continuum model of the electronic bands in MA-tBLG, for an analysis of the matrix structure of polarization operators, for a study of the dielectric function $\varepsilon(q)$ in different dielectric environments, for a discussion of the temperature dependence of the polarization functions, and for investigations of the dependencies of internal screening on twist angles, doping, interlayer coupling parameters, and energy gaps in the electronic excitation spectrum.
[43] S. V. Vonsovsky and M. I. Katsnelson, *Quantum Solid-State Physics* (Springer, Berlin, 1989).
[44] F. Aryasetiawan, M. Imada, A. Georges, G. Kotliar, S. Biermann, and A. I. Lichtenstein, Phys. Rev. B **70**, 195104 (2004).
[45] E. G. C. P. van Loon, H. Hafermann, A. I. Lichtenstein, A. N. Rubtsov, and M. I. Katsnelson, Phys. Rev. Lett. **113**, 246407 (2014).
[46] Figure 3 of Ref. [45] shows that the spectral weight in the loss function $\mathrm{Im}\,1/\epsilon$ is suppressed when going into a Mott state, particularly in the important long-wavelength and low-energy region. This suppression of spectral weight implies that

screening by the correlated bands is strongly suppressed in a Mott insulating state.

[47] A study of the full matrix structure of $\Pi_0^{\mathbf{G},\mathbf{G}'}$ is given in the Supplemental Material [42]. The diagonal matrix elements of $\Pi_0^{\mathbf{G},\mathbf{G}'}$ are by far the largest at all $\mathbf{q}$ in cRPA and also leading in RPA except for certain $\mathbf{q}$ close to the mini-BZ boundaries. Here, we analyze the diagonal matrix elements $\mathbf{G} = \mathbf{G}'$ by considering the single element $\Pi_0 \equiv \Pi_0^{\mathbf{G}=\mathbf{G}'=\mathbf{0}}$ and allowing for $\mathbf{q}$ to run out of the first mini-BZ in the sense of an extended zone scheme.

[48] M. I. Katsnelson, *Graphene: Carbon in Two Dimensions* (Cambridge University Press, Cambridge, UK, 2012).

[49] X. L. Yang, S. H. Guo, F. T. Chan, K. W. Wong, and W. Y. Ching, Phys. Rev. A **43**, 1186 (1991).

[50] E. H. Hwang and S. Das Sarma, Phys. Rev. Lett. **101**, 156802 (2008).